Biochemistry

Article

pubs.acs.org/biochemistry

Structural Stability of the Coiled-Coil Domain of Tumor Susceptibility Gene (TSG)-101

Jordan T. White, Dmitri Toptygin, Randy Cohen, Natalie Murphy, and Vincent J. Hilser*

Department of Biology, Johns Hopkins University, 3400 North Charles Street, Baltimore, Maryland 21218, United States

Supporting Information

ABSTRACT: The tumor susceptibility gene-101 coiled coil domain (TSG101cc) is an integral component of the endosomal maturation machinery and cytokinesis, and also interacts with several transcription factors. The TSG101cc has been crystallized as a homotetramer but is known to interact with two of its binding partners as a heterotrimer. To investigate this apparent discrepancy, we examined the solution thermodynamics of the TSG101cc. Here, we use circular dichroism, differential scanning calorimetry, analytical ultracentrifugation, fluorescence, and structural thermodynamic analysis to investigate the structural stability and the unfolding of the TSG101cc. We demonstrate that TSG101cc exists in solution primarily as a tetramer, which unfolds in a two-state manner. Surprisingly, no homodimeric or homotrimeric species were detected. Structural thermodynamic analysis of the homotetrameric structure and comparison with known oligomeric coiled-coils suggests that the TSG101cc homotetramer is comparatively unstable on a per residue basis. Furthermore, the homotrimeric coiled-coil is predicted to be much less stable than the functional heterotrimeric coiled-coil in the endosomal sorting complex required for transport 1 (ESCRT1). These results support a model whereby the tetramer−monomer equilibrium of TSG101 serves as the cellular reservoir of TSG101, which is effectively outcompeted when its binding partners are present and the heteroternary complex can form.

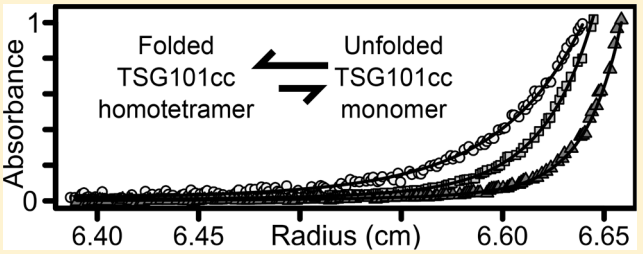

Tumor susceptibility gene-101 (TSG101, yeast homologue vps23) is a protein with multiple roles in eukaryotic biology. As a member of the endosomal sorting complex required for transport 1 (ESCRT1), TSG101 recruits other proteins to maturing endosomes and assists in the formation of multivesicular bodies[1−3] and many budding viruses.[4] TSG101 is also involved in cytokinesis,[5] and in mammals, TSG101 can act as a transcriptional regulator.[6] The numerous roles of TSG101 are facilitated through its four domains (Figure 1): The N-terminal UEV domain recruits TSG101 to membrane proteins targeted for degradation,[7] the proline-rich region recruits TSG101 to the cytokinetic furrow,[5] the coiled-coil assembles most of the ESCRT1 complex,[8] and the steadiness (i.e., stability) box plays a role in forming the bridge between the ESCRT1 and ESCRT2 complexes.[8,9] Of these, the coiled-coil domain is also of significance in transcriptional regulation, as it is believed to interact with several transcription factors.[6,10] In spite of the growing body of literature identifying novel binding partners and previously unknown functions of TSG101, there is an incomplete picture regarding the structural thermodynamics of the TSG101 coiled-coil and its role in modulating the stoichiometry of interaction.

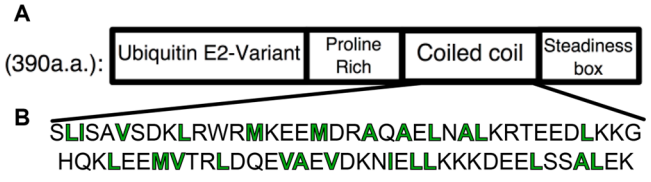

Figure 1. Schematic of TSG101 domain organization. (A) The domains pictured here are scaled to their length and the domain of interest is expanded in (B) The coiled-coil construct used in this study comprises amino acids 229−304 of the native sequence (76 amino acids long plus 2 a.a. left by the N-terminal tag). Hydrophobic residues are colored green.

The coiled-coil of TSG101 (TSG101cc) has been crystallized as a homotetramer (PDB 3iv1), but its oligomerization state has yet to be established in solution. This issue is significant because contrary to the tetrameric form observed for TSG101cc in isolation, the solution and crystal structures of the ESCRT1 coiled-coil are heterotrimers of TSG101/vps23 (yeast homologue) and two binding partners.[8,11] We note that other coiled-coils have been shown to adopt different structures or oligomeric states in crystal and in solution form.[12,13] Furthermore, ongoing studies in our lab suggest TSG101cc can also form a heterodimer, with the human glucocorticoid receptor (to be published elsewhere). Biological regulation through the modulation of the oligomeric state of a protein has been reported in a number of other systems (morpheein proteins[14]), including oligomerization of helix−loop−helix and

Received: May 16, 2017
Revised: July 20, 2017
Published: August 4, 2017

DOI: 10.1021/acs.biochem.7b00469
Biochemistry 2017, 56, 4646−4655

coiled-coil peptides, interactions in the mothers-against-decapentaplegic family of proteins, the hepatitis B viral capsid protein, and porphobilinogen synthase among others.[15−20] Here, we set out to determine the oligomeric state of TSG101cc in solution and to determine whether its oligomeric state is functionally modulated.

We show that TSG101cc in solution exists primarily as a tetramer that is in equilibrium with unfolded monomers. Despite the ability of TSG101cc to form heterotrimeric coiled-coils, no measurable homotrimeric (or homodimeric) species were observed. Thermal unfolding of TSG101cc as a function of protein concentration and pH provided access to the thermodynamic mechanism of stabilization of the tetramer. Furthermore, structural thermodynamic analyses of the TSG101cc tetramer and ESCRT1cc heterotrimer illuminates the structural basis of the tetramer stability and provides insight into the role of the homotetramer in regulating its hetero-oligomeric function.

MATERIALS AND METHODS

Protein Expression and Purification. The sequence of our expression construct spans amino acids 229−304 of TSG101 (Figure 1, Supporting Information, UniProt: Q99816). On the N-terminus is a 9xHis tag, followed by a TEV protease cleavage site and an extra serine. Competent BL21 DE3 pLysS cells were made in house and used for expression (Novagen strain). Growth proceeded in LB medium, with a 1 mM IPTG induction at an $O.D._{600}$ 0.6−1.2, followed by growth at 37 °C for 4 h or overnight at 16 °C. Little difference in expression was observed under these conditions. Cells were pelleted, washed with PBS, and lysed by sonication (20 mM Tris, 6 M Gdn, 20 mM imidazole, 500 mM NaCl, pH 8). After clearing of the lysate at 15 krpm for an hour, the lysate was purified using Ni-NTA. The His tag was cleaved off using TEV protease, and protein was passed over an anion exchange column followed by Ni-NTA. At this point TSG101cc was a single band by SDS-PAGE.[21] For differential scanning calorimetry (DSC), protein was purified further using size exclusion chromatography (SEC, HiLoad 16/600 Superdex 75 pg, GE).

For pyrene labeled protein, which was used only in analytical ultracentrifugation and fluorescence (Supporting Information), we utilized PMIA (*N*-(1-pyrenemethyl) iodoacetamide; Setareh biotech). Quikchange PCR was used to change a serine to a cysteine in our expression construct (Supporting Information). The serine in question is part of the N-terminal tag, not the native TSG101 sequence. This protein was purified as described above, dialyzed to labeling buffer (50 mM HEPES and 1 mM TCEP at pH 7.3), then labeled for 1 h at room temperature using 10 mol equiv of PMIA, relative to moles of protein, dissolved in DMSO. For efficient labeling, it was found that ∼5% DMSO was required in the final reaction mixture. Labeling was quenched using 10 mol equiv of DTT, relative to the moles of PMIA. This resulted in a turbid solution that was 0.2 μm filtered, then separated using SEC.

The first peak of SEC was consistently a mixture of TSG101cc with one or as many as three pyrene labels, as determined by mass spectrometry (Supporting Information). Iodoacetamide is known to react with amines, and attempts to prevent this by pH optimization did not succeed. However, the second peak we observed from SEC was consistently a mixture of singly labeled (∼66−80%) and unlabeled protein. This is what was used in all analytical centrifugation and fluorescence experiments described here.

The concentration of unlabeled protein was determined by its absorbance at 280 nm in guanidine, $\varepsilon_{TSG101cc}$ = 5690 M^{-1} cm^{-1}.[22] The concentration of PMIA labeled protein was determined by its absorbance at 345 nm (44 700 M^{-1} cm^{-1} Setareh Biotech). For PMIA labeled protein, extinction coefficients at other wavelengths were set relative to the 345 nm pyrene peak.

Circular Dichroism (CD). For CD measurements, protein was dialyzed to 20 mM Na_2HPO_4 plus 50 mM NaCl and pH adjusted with HCl (6.7, 7.2, 7.5). All CD data shown here were gathered using an Aviv CD spectrophotometer and a 1 mm path length, quartz cuvette. Each wavelength scan was in 1 nm increments, with a bandwidth of 1 nm, from 250 to 195 nm. The thermal melt data shown are with 1 °C increments and a 2 min incubation at each step. All CD data were averaged for five seconds at each measurement and buffer signal was subtracted. Reversibility (often between 70 and 96%) was determined by remeasuring the signal at 222 nm and 20 °C. We obtained our best data by diluting the protein several hours beforehand and degassing the protein for 5 min before measurement.

Differential Scanning Calorimetry (DSC). Protein was dialyzed to 20 mM PIPES and 200 mM NaCl and pH adjusted with NaOH (6.7, 7.2, 7.5). Data were collected with a microCal DSC at a scan rate of 1.5 °C per minute and duplicated with independent protein preparations and at least two scans. Repeated scanning of TSG101cc was highly reversible (∼99% refolded) as long as the final temperature was ≤ ∼73 °C (346 K). The data shown here have been scan rate normalized, buffer subtracted, and then normalized to the total concentration of monomeric protein. To circumvent baseline uncertainty in the native region that rendered determination of ΔC_p problematic, the ΔC_p was held constant at a value of 690 cal per K·mol of monomer based on the COREX analysis.

Analytical Ultracentrifugation (AUC). PMIA-labeled protein was dialyzed to 20 mM HEPES, 200 mM NaCl, and 1 mM TCEP and adjusted to a pH of 7.2 using NaOH. Data were collected at initial concentrations of 5, 9, and 18.2 μM pyrene-labeled TSG101cc, and the samples were loaded into epoxy centerpieces with sapphire windows (Spin Analytical). The Beckman XL-I was set to take absorbance measurements at 329, 336, and 345 nm. The three rotor speeds used were 29, 37, and 44 krpm, and final equilibrium took about 18 h per rotor speed. The data were fit globally with several models using HeteroAnalysis (JL Cole and JW Lary of University of Connecticut Bioservices Center). Partial specific volume and solvent density were calculated using SEDNTERP (J Philo). The data were replicated using a separate protein preparation that yielded fitted values within error of those presented here.

COREX/BEST Calculations. Per-residue stability analysis of TSG101cc proceeded in a manner largely described before for other proteins.[23−25] In this work, we used a window size of eight residues and 100 000 Monte Carlo simulations per partition. The entropy weighting factor was set to 1.029 to make the maximal residue stability roughly match our CD data at 150 μM protein and a pH of 7.2. We used H++ to calculate pK_a's for titratable residues, and used this as input for a pH dependent COREX/BEST calculation.[26] Solvent accessible surface area calculations were made with a 1.4 Å rolling ball from a subroutine of COREX,[27] and subsequent thermodynamic analyses proceeded similarly to the manner described by others before.[28−30]

DOI: 10.1021/acs.biochem.7b00469
Biochemistry 2017, 56, 4646−4655

RESULTS

Circular Dichroism Reveals α-Helical Structure. Circular dichroism (CD) was used to investigate the secondary structure of TSG101cc. As Figure 2 reveals, and consistent with the crystal structure, TSG101cc is indeed highly α-helical at low temperatures, as indicated by the strong peaks in negative ellipticity at 208 and 222 nm. Heating of the TSG101cc from 4−68 °C (Figure 2) resulted in a thermally induced conformational transition in which the α-helical content was lost, giving way to a CD spectrum that is essentially invariant above 56 °C and which corresponds to the expected spectrum of a disordered polypeptide (Figure 2). Analysis of the temperature-dependent transition reveals an isodichroic point at ∼204 nm, which suggests that the thermal transition, to a first approximation, involves just two states. Consistent with this observation, further analysis of the temperature dependence of the CD spectra using singular value decomposition (SVD)[31,32] reveals that just two singular values can explain 97.7% of the variation in the data (Supplementary Figure 5).

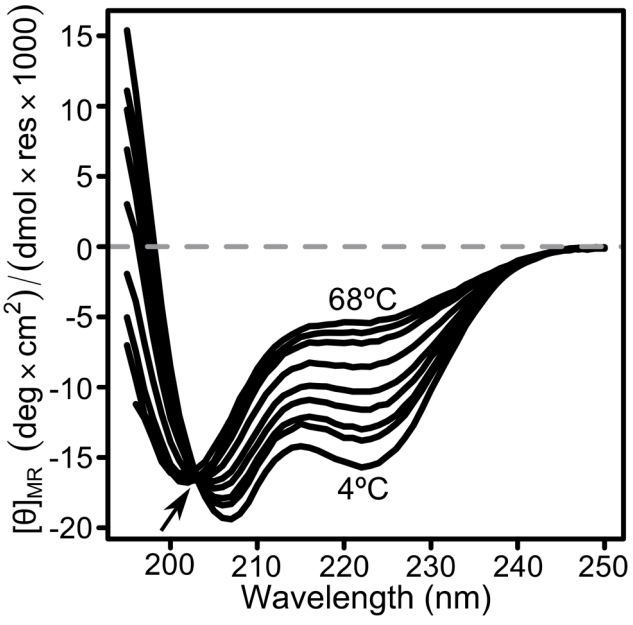

Figure 2. Circular dichroism wavelength scan of a temperature melt of TSG101cc. The data have an iso-dichroic point at ∼204 nm, highlighted by the arrow. This particular data set is from 24 μM protein that refolded to 72% of its original signal at 20 °C. The start (4 °C) and end (68 °C) point temperatures are labeled. The intermediate temperatures after 4 °C: 14°, 20°, 26°, 32°, 38°, 44°, 50°, 68 °C. Two temperatures, 56° and 62 °C, are omitted for clarity because they overlapped with the 68° scan.

To determine whether changes in the degree of oligomerization are associated with the conformational transition, thermal unfolding experiments were performed at various protein concentrations.[33,34] The data were fit globally with respect to temperature, concentration, and pH using the following two-state, simultaneous dissociation, and unfolding scheme:

$$N_n \overset{K}{\leftrightarrow} n^*U \quad (1)$$

where N_n is the folded oligomer, n is the stoichiometry, K is the equilibrium constant, and U is the unfolded monomer (see the Supporting Information for derivation of the associated equations[35]).

As Figure 3 reveals, both protein concentration and pH affect the temperature dependence of the mean residue ellipticity ($[\theta]_{MR,\ 222\ nm}$). The increase in apparent transition temperature (T_m) with concentration reveals that unfolding decreases the degree of oligomerization. The shift of the apparent T_m (for a given protein concentration) to lower temperatures with increasing pH suggests that the α-helical oligomeric state binds protons more tightly than the unfolded state. Specifically,

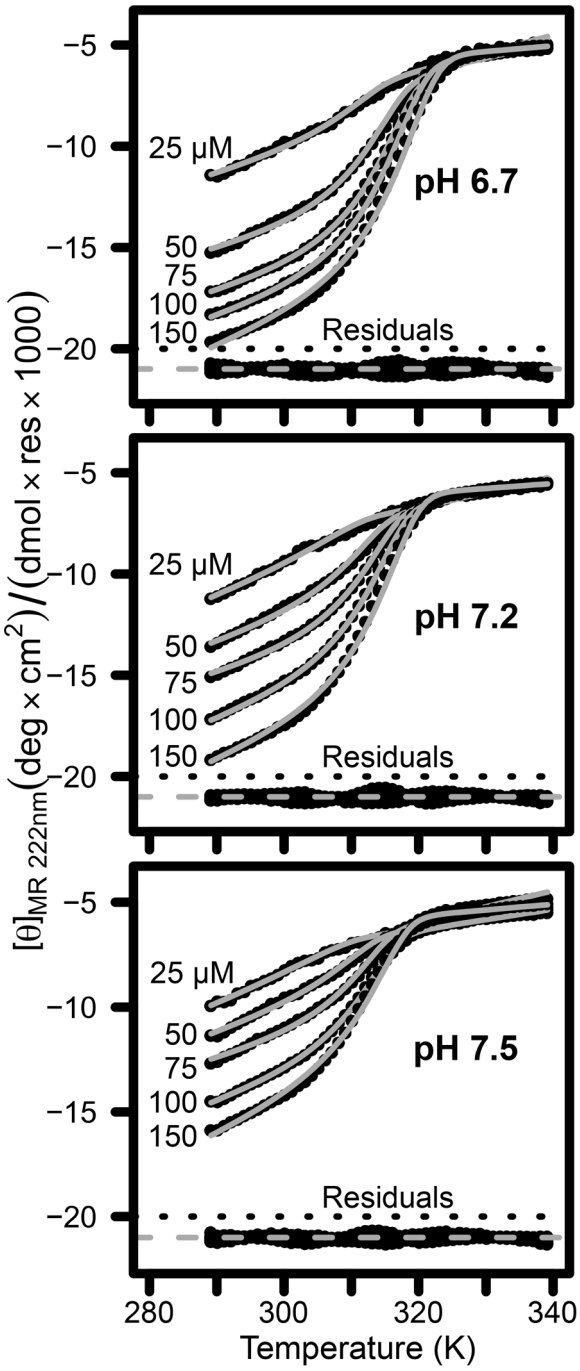

Figure 3. Circular dichroism thermal melt at multiple pH's and concentrations. μM concentrations and pH are marked alongside each data set. The best fits are plotted over the data points and the residuals are plotted below each data set. Refolding for 10 min at 20 °C yielded 70−96% of the original signal.

DOI: 10.1021/acs.biochem.7b00469
Biochemistry 2017, 56, 4646−4655

the average number of protons lost upon unfolding the protein can be determined using the expression:[36]

$$\Delta n = \left(\frac{dT^\circ}{dpH}\right) * \frac{\Delta H^\circ}{2.303 * R * (T^\circ)^2} \quad (2)$$

where Δn is the change in the number of protons bound and dT°/dpH is the slope of a plot of T° versus pH. The data indicate a loss of ~0.6 protons by each monomer upon unfolding, which corresponds to ~2 protons per tetramer. The global fit of the data according to a two-state (folded tetramer to unfolded monomer) transition produced the parameters shown in Table 1.

Table 1. Fitted Thermodynamic Values for CD[a]

pH	T° Kelvin	ΔH° kcal/mol	ΔC_p cal/(mol*K)	average $\Delta n_{protons}$ calculated
6.7	350.4 ± 3.4	56.5 ± 9.8	675 ± 421	−0.64
7.2	347.1 ± 3.4			−0.65
7.5	345.4 ± 3.4			−0.66

[a]Five concentrations from 25 to 150 μM were used at each pH. Globally fitted values are presented with 95% confidence intervals of the fit and are with respect to moles-monomer. The change in protons bound was calculated with eq 2. We note that ΔC_p was determined from the temperature dependence of ΔH obtained at the different pH values. The fitted ΔH° is the intrinsic enthalpy of unfolding where $\Delta S_{translation} = 0$, and is thus shared for all pH values.

Differential Scanning Calorimetry (DSC). To further analyze the thermodynamics associated with the thermally induced unfolding-dissociation transition, DSC was performed on TSG101cc as a function of concentration and pH. Because DSC directly monitors the heat associated with the thermally induced transition, it is unique among experimental approaches in that it provides direct access to the partition function (i.e., the significantly populated states and their respective energies). Specifically, the unfolding and dissociation of an oligomeric protein N_n will be reflected in the shape of a DSC curve. Increasing n will cause an increase in the asymmetry and sharpness of a DSC curve,[35] and increasing the number of states will cause broadening and/or extra peaks.[37]

Consistent with the results obtained from CD, analysis of the DSC thermograms reveals that TSG101cc exists as a tetramer that undergoes a cooperative unfolding/dissociation reaction with temperature (Figure 4). Also similar to the CD experiments, lower concentrations and higher pH values were found to destabilize the TSG101cc tetramer. Because the T_m concentration dependence is logarithmic, the concentration-induced T_m shifts in Figure 4 are subtler than those seen at the lower concentrations used in CD. Shown in Table 2 are the average values from individual fits of the DSC data, using the same equations derived for the CD analysis (Supporting Information). Importantly, the DSC data are in general agreement with the CD data.

Analytical Ultra-Centrifugation (AUC). Equilibrium AUC was also used to probe TSG101cc's oligomeric state. Thermal denaturation has the potential to conceal unstable intermediates, as the unfolded state rapidly increases in probability with increasing temperatures. Centrifugation of TSG101cc at 20 °C, however, allows us to challenge the findings obtained from CD and DSC. To increase the sensitivity to partially unfolded or different oligomeric states, TSG101cc was end-labeled with pyrene using a Cys residue incorporated into the N-terminal

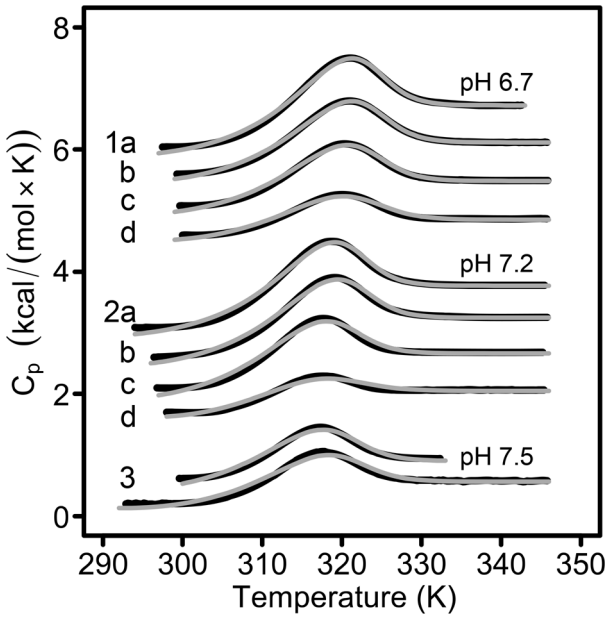

Figure 4. Differential scanning calorimetry of TSG101cc at various pH's and concentrations. All of these data are normalized to the moles of monomeric protein and offset vertically for visual purposes. Data are shown as black lines and the associated fits are gray lines. Concentration and pH are as follows: (1) pH 6.7 (a) and (b) 414 μM, (c) 295 μM, (d) 200 μM; (2) pH 7.2, (a) 590 μM, (b) 414 μM, (c) 295 μM, (d) 147 μM; (3) pH 7.5, both at 416 μM. Each scan was reproduced with nearly 99% of the protein refolding.

Table 2. Fitted Thermodynamic Values for DSC[a]

pH	T° Kelvin	ΔH° kcal/mol
6.7 (4)	358.9 ± 5.6	45.6 ± 1.6
7.2 (4)	356.7 ± 8.4	
7.5 (2)	355.9 ± 2.2	

[a]Data were fit individually and averages of the fits are presented ± two standard deviations. Enthalpy is with respect to moles-monomer. Parentheses indicate the number of independent experiments used in the fits and averaging. ΔC_p was held at a constant 690.085 (estimated by COREX). The fitted ΔH° is the intrinsic enthalpy of unfolding where $\Delta S_{translation} = 0$. See text for further description. The subtle shifts in T° prevented accurate determination of changes in proton binding.

tag (see Supporting Information for sequences, mass spectrometry, and fluorescence), and detection was facilitated with absorbance optics.

Shown in Figure 5 is a representative AUC trace at 9 μM. A two-state fit of the data reveal a monomer−tetramer equilibrium that is consistent with the CD and DSC results: MW = 9778 ± 295 Da, stoichiometry = 3.97 ± 0.11, $\ln(K_d)$ = −39.41 ± 1.51, $K_d = 7.66 \times 10^{-18}$ M^3, RMSD = 0.01003. Of note is that a one-state fit is inconsistent with the known monomeric mass (~9313 Da monomeric mass by MALDI, see Supporting Information) and produces skewed residuals at higher rotor speeds (MW = 35775 ± 102 Da, RMSD = 0.01101). Similarly, a three-state fit was precluded as it produced no justifiable improvement of the residuals over the two-state fit. Importantly, the K_d, as measured by AUC corresponds to a stability of 23.0 ± 0.9 kcal/mol-cooperative unit at 20 °C, which is consistent with our thermal measurements (CD at pH 7.2 and 20 °C ΔG = 23.2 kcal/mol-oligomer, and DSC ΔG = 15.8 kcal/mol-oligomer). The agreement between the DSC, CD, and AUC measurements

DOI: 10.1021/acs.biochem.7b00469
Biochemistry 2017, 56, 4646−4655

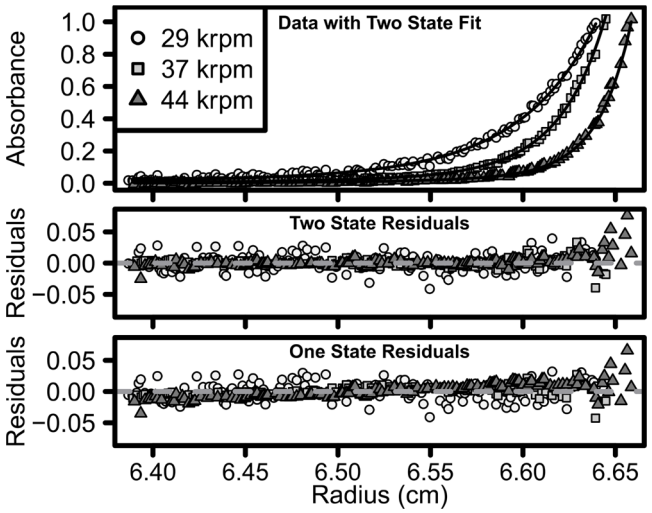

Figure 5. AUC of the TSG101cc. The top panel is baselined data from a channel loaded with 9 μM TSG101cc-pyrene. Data are points and two-state fits are black lines. The lower two panels are residuals from two and one state fits, respectively. Note that at higher rotor speeds, the residuals are tilted in the one-state case. The absorbance shown is for 329, 330, and 329 nm at 29, 37, and 44 krpm, respectively.

strongly suggests that under native and denaturing conditions, no appreciable amount of oligomers other than tetramer are populated.

Structural Thermodynamic Analysis Using COREX/BEST. To investigate the structural stability of TSG101cc, the crystal structure of the tetrameric complex was analyzed using the COREX/BEST algorithm.[38,39] COREX/BEST uses the high-resolution structure as a template from which to derive an ensemble of partially unfolded states. The fundamental assumption in the COREX algorithm is that conformational fluctuations can be modeled as local unfolding, and that the folded regions in each state can be represented by the high-resolution structural coordinates. Different states are generated by systematically unfolding all regions (in eight residue windows) of the protein in all combinations, thus producing an ensemble that ranges from the fully unfolded state, in which all regions are unfolded, to the fully folded state, in which no regions are unfolded. The energetics were determined using the well-established calorimetric parametrization of the enthalpy and heat capacity as described elsewhere.[39−46]

The output of COREX/BEST is a profile of the residue-specific stability of the molecule, which is presented from the N to C terminus (Figure 6A). Because COREX/BEST generates an ensemble, the residue-specific stability is described at every position by the expression:

$$\kappa_{f,j} = \frac{\sum P_{f,j}}{\sum P_{nf,j}} \quad (3)$$

where the stability at any position j is simply the ratio of the summed probability of all states wherein residue j is in a folded region, to the summed probability of states wherein that residue is in a nonfolded region. As such, high stability constants (i.e., $RT \ln[\kappa_f]$) correspond to regions where the probability of states wherein residue j is folded is high, while lower stability constants are found in regions where the probability of states wherein residue j is not folded is high. Importantly, the stability constants determined by COREX/BEST can be compared with the protection factors obtained from hydrogen exchange

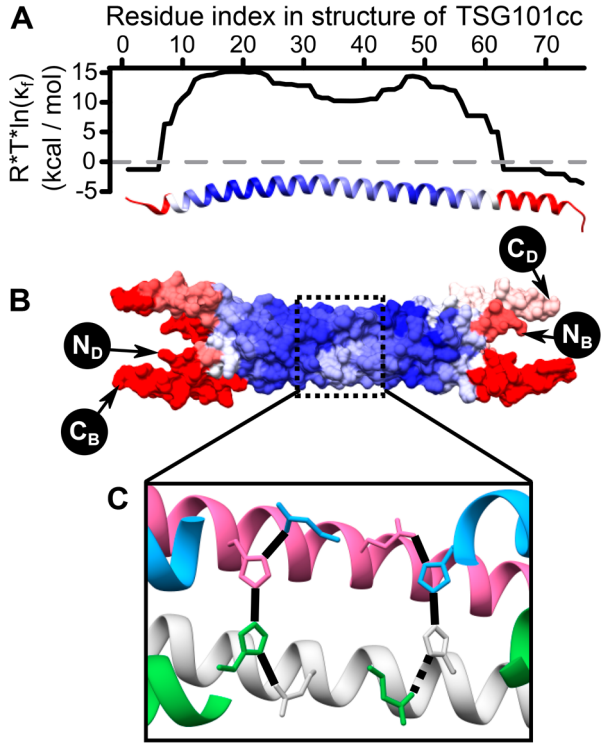

Figure 6. (A) COREX/BEST residue stability analysis for chain A of pdb: 3iv1, at pH 7 and 293.15 K. The y-axis is the energy of unfolding a given residue on the x-axis. Laid horizontally from N to C-terminus is chain A from the tetramer structure, depicted as a ribbon. A gray dashed line indicates an energy of 0 and was used as the upper limit for the red coloring of the structure. The upper limit for blue coloring was +15. (B) The molecular surface of the TSG101cc tetramer is colored here as above. The N and C-termini of chains B and D are labeled to highlight the antiparallel nature of the tetramer ("N_B" etc.). (C) Zoom in of the proposed H-bond network is shown with residues E262 and H269 of all the chains. The H-bonds predicted by Chimera are shown as solid lines, except one with relaxed constraints as a dashed line. Chain A = light gray, chain B = green (cut away), chain C = pink, chain D = blue (cut away).

experiments under conditions where protection reports on a stability (i.e., under EX2 conditions). The excellent agreement between COREX and a test set of proteins suggests that the regional differences in stability determined from COREX are meaningful.[47]

Analysis of the COREX results for TSG101cc reveals two important features. First, both ends of the homotetrameric coiled coil are predicted to be unstable and largely disordered in solution (Figure 6A,B). This is consistent with the fact that the ends of each chain are not in contact with one another in the high-resolution structure, and thus lack the interhelix stabilization that is characteristic of coiled-coils.[34,48] Such fraying of coiled-coil ends has been observed in other proteins.[49,50] Second, the central portion of the coiled-coil is predicted to be highly stable, which is consistent with the high degree of interhelical surface buried between the individual monomers in the coiled-coil.

A slight decrease in the stability of the central portion of the coiled-coil region is also observed. This decrease is accompanied by an increase in the residue−specific conformational entropy of unfolding of the central portions of the TSG101cc. The increased conformational entropy and decreased stability is in part related to the presence of a glycine (Gly) residue in the

DOI: 10.1021/acs.biochem.7b00469
Biochemistry 2017, 56, 4646−4655

center of the helix (Gly268, which is a.a. 40 in Figure 6A, see Supplementary Figure S6) which increases the conformational entropy of states wherein Gly268 is unfolded, thus destabilizing helical states by ∼1.0 kcal/mol. Indeed, it is this destabilizing conformational entropic effect that largely accounts for the infrequency of Gly residues within helices of folded, globular proteins.[40]

We note the presence of Gly at position 268 is immediately followed by His 269, which is part of an interhelical H-bond network involving Glu262 of chain A, His269 of chain B, His269 of chain C, and Glu262 of chain D, all of which are observed in the X-ray structure (Figure 6C) (and which are predicted to be hydrogen bonded using the program Chimera[51]). We also note that the two H-bonding networks per tetramer would, upon dissociation, release one proton per each histidine pair, producing a net release of two protons per tetramer, a value that is in good quantitative agreement with our experimental results. Interestingly, such an H-bond network could also play a role in setting the register and orientation of the coiled-coil, as seen in some other natural and engineered coiled-coils.[52,53]

A more detailed analysis of the COREX/BEST results provides access to the thermodynamic mechanism underlying the homotetramer stability. COREX calculates the unfolding energetics based on changes in solvent accessible apolar (ΔASA_{ap}) and polar (ΔASA_{pol}) surface area between states, from which ΔC_p, $\Delta H_{solvation}$, and $\Delta S_{solvation}$ can be determined.[23] Two other components of the entropy change can also be determined: The conformational entropy, $\Delta S_{conformation}$ can be calculated based on backbone and side chain rotomers, as described previously,[40,54] and the translational and rotational entropy, $\Delta S_{translation}$, for each oligomeric state can be calculated given the stoichiometry.[55]

Table 3 contains the structural thermodynamic analyses of the TSG101cc homotetramer as well as the intermediate oligomeric states, generated in silico by deletion of excess chains. The calculated ΔG_{total} and ΔC_p for the tetramer are in agreement with the values measured experimentally (COREX: 5.2 kcal/mol-monomer and ∼650−690 cal/K/mol-monomer, respectively), suggesting the algorithm adequately captures the underlying thermodynamic basis of TSG101cc stabilization. Inspection of the detailed mechanism reveals that the major determinant of the stability of the tetramer is the apolar surface buried in the binding interface between helical monomers. Specifically, the burial of apolar versus polar surface area (on a per residue basis) is significantly higher for the tetramer than for the trimer, dimer, or monomer (1.2-, 1.6-, 2.5-fold more ΔASA_{ap} in the tetramer, respectively). Of note is that the lower order oligomers are predicted by COREX/BEST to be significantly less stable than the homotetramer, which is also consistent with the experimental results.

Table 3. Structural Thermodynamic Analysis of the TSG101cc at 20 °C (293.15 K)[a]

parameter	monomer	dimer	trimer	tetramer
ΔASA_{Apolar} (Å^2)	1331	2105	2776	3382
ΔASA_{Polar} (Å^2)	2645	2834	3077	3345
ΔC_p (cal/K mol)	−88	211	449	652
$\Delta H_{generic}$ (kcal/mol)	75.5	63.0	55.5	50.8
ΔS_{solv} (cal/K mol)	−70	−158	−232	−297
ΔS_{conf} (cal/K mol)	390	420	429	449
$\Delta G_{generic}$ (kcal/mol)	−18	−13.7	−2.26	6.11
ΔG_{trans} (kcal/mol)	0	−0.77	−0.92	−0.95
ΔG_{total} (kcal/mol)	−18	−14	−3.2	5.2

[a]All values are relative to moles of monomer and refer to the unfolding reaction. Note that the tetramer ΔG_{total} calculated here is close to the values we measured experimentally (CD = 5.8, DSC = 4.0, AUC = 5.7 kcal/K·mol-monomer). The translational energy of dissociation was calculated as in ref 55.

To estimate the relative stability of the TSG101cc heterotrimer, a structural analysis of the yeast ESCRT1 coiled-coil (pdb: 2p22) was also performed.[8] The results reveal a binding interface that is 77% apolar, compared to 75% for the TSG101cc homotetramer (Tables S2 and S3, respectively). Analysis of the results (Table S2) also reveals the stability of the ESCRT1 coiled-coil fragment to be similar to the TSG101cc homotetramer, suggesting that under such conditions the relevant equilibrium would involve TSG101cc homotetramer, unfolded TSG101cc monomer and ESCRT1 heterotrimer, with no appreciable accumulation of the other TSG101cc homo-oligomeric species. Consistent with our results, experimental analysis of the full-length ESCRT1 complex revealed that it sediments as a tightly bound, single species in AUC.[8,11]

Finally, to establish context for the TSG101cc analysis presented here, we also compared our results to other oligomeric proteins, including five other coiled-coils. As Table S3 reveals, the packing of hydrophobic residues is not unique to the TSG101cc. Although our results reveal a similar amount of hydrophobic surface buried in other coiled-coil interfaces, TSG101cc is less stable (i.e., lower $T°$) than most other mesophilic, oligomeric proteins, with the difference arising from the accumulation of small differences in polar free energy and conformational entropy. In short, although TSG101cc has clearly not evolved to populate homotrimeric and homodimeric states, it also does not appear to have evolved to strongly homotetramerize, as both the calculations and our experimental results clearly reveal.

DISCUSSION

In this study, we set out to understand the oligomerization of the human TSG101cc in solution. In isolation, we find that the coiled-coil domain significantly populates only two states, a homotetramer and a monomer. Our thermodynamic analysis indicates that the intermediate homo-oligomeric states would likely be unstable because hydrophobic packing present in the homotetrameric interactions is missing in the homotrimer/dimer. This has broader implications and immediately suggests that TSG101cc interacts with its binding partners via large, hydrophobic interactions, a supposition that is supported by thermodynamic analysis of the ESCRT1 coiled-coil. Without significant hydrophobic interactions, hetero-oligomers would be unstable relative to the TSG101cc homotetramer.

We also found that the TSG101cc tetramer releases ∼2.0 protons per tetramer upon unfolding. This is consistent with our analysis of the homotetramer structure (pdb: 3iv1). The four histidine residues at position 269 would likely release two protons upon unfolding of the tetramer producing 0.5 protons per monomer. It is unclear why the TSG101cc evolved to be stabilized as pH is lowered, although we do note that cellular pH can vary from ∼5.7—7.4 depending on various cellular states.[56−61] Determining if these subtle pH changes affect TSG101 function in vivo awaits further study.

Lastly, we find that the tetramer of the TSG101cc is relatively unstable. Compared to the other tetramers (Table S3),

DOI: 10.1021/acs.biochem.7b00469
Biochemistry 2017, 56, 4646−4655

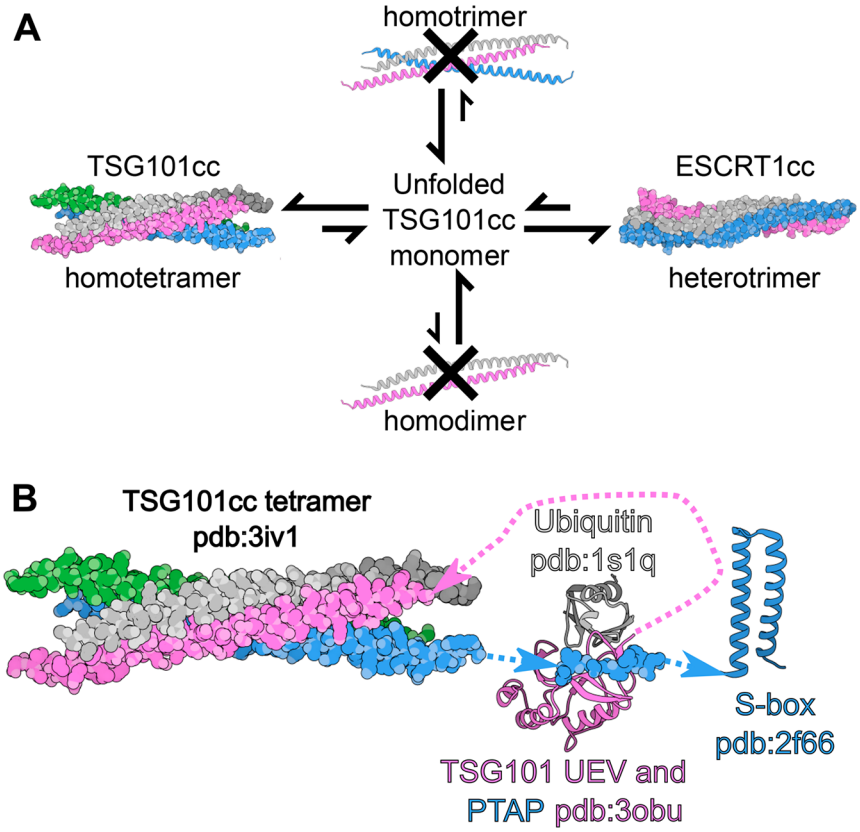

Figure 7. (A) Reaction scheme depicting the main discoveries of this work. On the left, each chain of the TSG101cc tetramer is depicted as atom spheres with carbons in darker colors than the other atoms (pink, gray, green, blue). At the top and bottom, the TSG101cc is depicted as a ribbon in the same colors. On the right, the TSG101cc homologue, vps23, is blue (vps27 is gray and mvb12 is pink, adapted from pdb: 2p22). The arrows are based on structural thermodynamic analyses, presented here, and experimental data presented here for TSG101cc or elsewhere for ESCRT1.[8,11] (B) The proposed structural model for the TSG101 tetramer. Each chain of the coiled-coil tetramer is depicted as in part A of this figure. The N-terminal UEV domain of the pink chain is depicted as a ribbon,[64] and was docked[69] to the TSG101 PTAP sequence of the blue chain (the original PTAP in pdb: 3obu is the HIV sequence, with little difference). The structure of the UEV domain bound to ubiquitin[68] was aligned with pdb: 3obu, and ubiquitin is colored dark gray; note that the PTAP motif does not occlude ubiquitin binding. The C-terminal S-box of the blue TSG101cc chain is depicted as a ribbon.[70] Unstructured regions are shown as dashed lines with arrows going from N to Ctermini. There would be three other UEV domain:PTAP interactions not shown here.

TSG101cc has the lowest $T°$ and the second lowest $\Delta G°_{20\ °C}$. This suggests that the unfolded monomer plays a thermodynamically significant role in the functional equilibrium. Even at some of the highest TSG101cc concentrations at pH 7.2, the TSG101cc unfolding curve begins in a physiological temperature range. At more physiological concentrations, the apparent T_m of unfolding is ~37 °C or lower, suggesting that the reservoir of TSG101cc is a balance of monomer and tetramer. Importantly, because the monomer−tetramer equilibrium is poised near the midpoint, it is most sensitive to concentration changes, meaning that any TSG101 that is sequestered by the ESCRT complex would be readily replenished by a shift in the tetramer to monomer equilibrium. The fact that the stability appears to be tuned by the presence of the conserved residues E262, G268, and H269 (and the corresponding interchain H-bond network) suggests that functional equilibrium is subject to fine-tuning from both pH and concentration changes.

While the TSG101cc by itself is weakly stable, we hypothesize that other interactions in full-length TSG101 may stabilize a homotetramer. It has been known for over a decade that the N-terminal, UEV domain of TSG101 binds a short peptide motif, P(S/T)AP, that is present in many animal and viral proteins that bind TSG101.[62−64] C-Terminal to the coiled-coil of TSG101 is a PTAP motif that can bind the TSG101 UEV domain.[65,66] At the time of its discovery, Pornillos and colleagues proposed that each TSG101 molecule looped around and bound itself—forming an autoinhibited state that other ESCRT proteins would be unable to bind. Here, we can add to this hypothesis by proposing that each TSG101 molecule engages in domain swapping in its tetrameric state (Figure 7B). Because every other strand of the coiled-coil runs antiparallel to its neighbors, the UEV domain of a neighboring strand could bind the C-terminal PTAP motif of an adjacent strand (Figure 7B).

Although the model hypothesized in Figure 7B is speculative, it does provide context to the results presented here and provides potential avenues for further study. The complex shown in Figure 7B would likely be highly stable and autoinhibited. Indeed, in vivo evidence does exist for an autoinhibited state of TSG101. Specifically, mutation of mouse TSG101's PTAP motif caused a precipitous increase in TSG101's association with the ESCRT0 protein, HRS, as determined by yeast two-hybrid.[67] In its natural context, TSG101 could take advantage of the homotetramer−monomer equilibrium to serve as the TSG101 reservoir, from which the ESCRT1 complex could draw. Local increases in concentration of TSG101 binding partners such as HRS[66] or ubiquitin[68] that both bind to the UEV domain of TSG101 could sequester

DOI: 10.1021/acs.biochem.7b00469
Biochemistry 2017, 56, 4646−4655

TSG101 monomers. In any event, the model proposed in Figure 7B reveals numerous possibilities for how TSG101 function can be affected by changes in stoichiometry, which can affect both inter- and intramolecular interactions, possibly in complex ways. For instance, to bind the TSG101 UEV domain, the HRS PSAP motif may have to displace the TSG101 PTAP motif. However, because it has been shown that the TSG101 PTAP binds its UEV domain approximately 1.5−fold better than does the HRS PSAP motif,[66] other domains are likely to play a role in mediating this interaction. Is it the case that binding of ubiquitin, for example, allosterically (or directly) destabilizes binding of the TSG101 PTAP motif, thereby releasing the UEV domain for binding to HRS? Although the answer to this question awaits further study, the fact that the concentration of available TSG101 monomer is within a tunable range suggests that dynamic availability of TSG101 may be a key determinant in HRS function.

CONCLUSION

In this work, we used solution and structural thermodynamics to define the oligomeric states of the TSG101 coiled-coil in vitro. We find evidence that TSG101cc evolved a highly cooperative association event that is stabilized by hydrophobic interactions and acidic pH, which gives us several clues as to how TSG101cc forms its hetero-oligomers not just with ESCRT1 but also with nuclear hormone receptors. The information gained here leads to new hypotheses that could inform future studies involving full-length TSG101 and its binding partners.

ASSOCIATED CONTENT

Supporting Information

The Supporting Information is available free of charge on the ACS Publications website at DOI: 10.1021/acs.biochem.7b00469.

Equations for CD, DSC, and fluorescence. Fluorescence data and methods. Supplemental Figures S1—6. Supplemental Tables S1—3 (PDF)

AUTHOR INFORMATION

Corresponding Author

*E-mail: hilser@jhu.edu. Tel: 410-516-6072. Fax: 410-516-5213.

ORCID

Vincent J. Hilser: 0000-0002-7173-0073

Author Contributions

J.T.W. designed experiments, purified protein, collected, and analyzed data. D.T. designed experiments, collected, and analyzed data. R.C. and N.M. performed experiments. V.J.H. designed experiments and analyzed data. J.T.W. and V.J.H. wrote the manuscript and all authors read the final manuscript.

Notes

The authors declare no competing financial interest.

ACKNOWLEDGMENTS

We thank Prof. E. Moudrianakis for advice and technical expertise with AUC. Prof. L. Brand for advice on fluorimetry experiments, Prof. E. Freire, for thermodynamic advice and Drs. A. Schoen, M. Rodgers, K. Tripp, and C. Sandlin, for technical advice. V.J.H. is supported by NIH grant GM063747 and NSF Grant MCB-0446050. J.T.W. was supported by the NIH Training Grant 5T32GM007231-39 to the Johns Hopkins University department of biology. R.C. current address is Rowan University School of Osteopathic Medicine, Stratford, NJ 08084. N.M. current address is Neuromuscular Diseases Research Section, Laboratory of Neurogenetics, NIA at NIH, Bethesda, MD 20892

REFERENCES

(1) Rothman, J. H., Howald, I., and Stevens, T. H. (1989) Characterization of genes required for protein sorting and vacuolar function in the yeast Saccharomyces cerevisiae. *EMBO J. 8*, 2057−2065.

(2) Robinson, J. S., Klionsky, D. J., Banta, L. M., and Emr, S. D. (1988) Protein sorting in Saccharomyces cerevisiae: isolation of mutants defective in the delivery and processing of multiple vacuolar hydrolases. *Mol. Cell. Biol. 8*, 4936−4948.

(3) Babst, M., Odorizzi, G., Estepa, E. J., and Emr, S. D. (2000) Mammalian tumor susceptibility gene 101 (TSG101) and the yeast homologue, Vps23p, both function in late endosomal trafficking. *Traffic 1*, 248−258.

(4) Morita, E., and Sundquist, W. I. (2004) Retrovirus budding. *Annu. Rev. Cell Dev. Biol. 20*, 395−425.

(5) Elia, N., Sougrat, R., Spurlin, T. A., Hurley, J. H., and Lippincott-Schwartz, J. (2011) Dynamics of endosomal sorting complex required for transport (ESCRT) machinery during cytokinesis and its role in abscission. *Proc. Natl. Acad. Sci. U. S. A. 108*, 4846−4851.

(6) Watanabe, M., Yanagi, Y., Masuhiro, Y., Yano, T., Yoshikawa, H., Yanagisawa, J., and Kato, S. (1998) A putative tumor suppressor, TSG101, acts as a transcriptional suppressor through its coiled-coil domain. *Biochem. Biophys. Res. Commun. 245*, 900−905.

(7) Katzmann, D. J., Babst, M., and Emr, S. D. (2001) Ubiquitin-dependent sorting into the multivesicular body pathway requires the function of a conserved endosomal protein sorting complex, ESCRT-I. *Cell 106*, 145−155.

(8) Kostelansky, M. S., Schluter, C., Tam, Y. Y., Lee, S., Ghirlando, R., Beach, B., Conibear, E., and Hurley, J. H. (2007) Molecular architecture and functional model of the complete yeast ESCRT-I heterotetramer. *Cell 129*, 485−498.

(9) Gill, D. J., Teo, H., Sun, J., Perisic, O., Veprintsev, D. B., Emr, S. D., and Williams, R. L. (2007) Structural insight into the ESCRT-I/-II link and its role in MVB trafficking. *EMBO J. 26*, 600−612.

(10) Muromoto, R., Sugiyama, K., Takachi, A., Imoto, S., Sato, N., Yamamoto, T., Oritani, K., Shimoda, K., and Matsuda, T. (2004) Physical and functional interactions between Daxx and DNA methyltransferase 1-associated protein, DMAP1. *J. Immunol. 172*, 2985−2993.

(11) Morita, E., Sandrin, V., Alam, S. L., Eckert, D. M., Gygi, S. P., and Sundquist, W. I. (2007) Identification of human MVB12 proteins as ESCRT-I subunits that function in HIV budding. *Cell Host Microbe 2*, 41−53.

(12) Gouda, H., Torigoe, H., Saito, A., Sato, M., Arata, Y., and Shimada, I. (1992) 3-Dimensional Solution Structure of the B-Domain of Staphylococcal Protein-a - Comparisons of the Solution and Crystal-Structures. *Biochemistry 31*, 9665−9672.

(13) Yan, Y., Winograd, E., Viel, A., Cronin, T., Harrison, S. C., and Branton, D. (1993) Crystal structure of the repetitive segments of spectrin. *Science 262*, 2027−2030.

(14) Jaffe, E. K. (2005) Morpheeins–a new structural paradigm for allosteric regulation. *Trends Biochem. Sci. 30*, 490−497.

(15) Fairman, R., Beran-Steed, R. K., Anthony-Cahill, S. J., Lear, J. D., Stafford, W. F., 3rd, DeGrado, W. F., Benfield, P. A., and Brenner, S. L. (1993) Multiple oligomeric states regulate the DNA binding of helix-loop-helix peptides. *Proc. Natl. Acad. Sci. U. S. A. 90*, 10429−10433.

(16) Breinig, S., Kervinen, J., Stith, L., Wasson, A. S., Fairman, R., Wlodawer, A., Zdanov, A., and Jaffe, E. K. (2003) Control of tetrapyrrole biosynthesis by alternate quaternary forms of porphobilinogen synthase. *Nat. Struct. Biol. 10*, 757−763.

DOI: 10.1021/acs.biochem.7b00469
Biochemistry 2017, 56, 4646−4655

(17) Stray, S. J., Ceres, P., and Zlotnick, A. (2004) Zinc ions trigger conformational change and oligomerization of hepatitis B virus capsid protein. *Biochemistry 43*, 9989−9998.
(18) Campbell, K. M., Sholders, A. J., and Lumb, K. J. (2002) Contribution of buried lysine residues to the oligomerization specificity and stability of the fos coiled coil. *Biochemistry 41*, 4866−4871.
(19) Jayaraman, L., and Massague, J. (2000) Distinct oligomeric states of SMAD proteins in the transforming growth factor-beta pathway. *J. Biol. Chem. 275*, 40710−40717.
(20) Apostolovic, B., and Klok, H. A. (2008) pH-sensitivity of the E3/K3 heterodimeric coiled coil. *Biomacromolecules 9*, 3173−3180.
(21) Candiano, G., Bruschi, M., Musante, L., Santucci, L., Ghiggeri, G. M., Carnemolla, B., Orecchia, P., Zardi, L., and Righetti, P. G. (2004) Blue silver: a very sensitive colloidal Coomassie G-250 staining for proteome analysis. *Electrophoresis 25*, 1327−1333.
(22) Edelhoch, H. (1967) Spectroscopic determination of tryptophan and tyrosine in proteins. *Biochemistry 6*, 1948−1954.
(23) Hilser, V. J., and Freire, E. (1996) Structure-based calculation of the equilibrium folding pathway of proteins. Correlation with hydrogen exchange protection factors. *J. Mol. Biol. 262*, 756−772.
(24) Whitten, S. T., Garcia-Moreno, E. B., and Hilser, V. J. (2005) Local conformational fluctuations can modulate the coupling between proton binding and global structural transitions in proteins. *Proc. Natl. Acad. Sci. U. S. A. 102*, 4282−4287.
(25) Pan, H., Lee, J. C., and Hilser, V. J. (2000) Binding sites in Escherichia coli dihydrofolate reductase communicate by modulating the conformational ensemble. *Proc. Natl. Acad. Sci. U. S. A. 97*, 12020−12025.
(26) Anandakrishnan, R., Aguilar, B., and Onufriev, A. V. (2012) H++ 3.0: automating pK prediction and the preparation of biomolecular structures for atomistic molecular modeling and simulations. *Nucleic Acids Res. 40*, W537−541.
(27) Motlagh, H. N., Toptygin, D., Kaiser, C. M., and Hilser, V. J. (2016) Single-Molecule Chemo-Mechanical Spectroscopy Provides Structural Identity of Folding Intermediates. *Biophys. J. 110*, 1280−1290.
(28) Murphy, K. P., and Freire, E. (1992) Thermodynamics of structural stability and cooperative folding behavior in proteins. *Adv. Protein Chem. 43*, 313−361.
(29) Boudker, O., Todd, M. J., and Freire, E. (1997) The structural stability of the co-chaperonin GroES. *J. Mol. Biol. 272*, 770−779.
(30) Todd, M. J., Semo, N., and Freire, E. (1998) The structural stability of the HIV-1 protease. *J. Mol. Biol. 283*, 475−488.
(31) Staskus, P. W., and Johnson, W. C., Jr. (1988) Conformational transition of hyaluronic acid in aqueous-organic solvent monitored by vacuum ultraviolet circular dichroism. *Biochemistry 27*, 1522−1527.
(32) Ionescu, R. M., Smith, V. F., O'Neill, J. C., Jr., and Matthews, C. R. (2000) Multistate equilibrium unfolding of *Escherichia coli* dihydrofolate reductase: thermodynamic and spectroscopic description of the native, intermediate, and unfolded ensembles. *Biochemistry 39*, 9540−9550.
(33) Johnson, C. R., Morin, P. E., Arrowsmith, C. H., and Freire, E. (1995) Thermodynamic Analysis of the Structural Stability of the Tetrameric Oligomerization Domain of P53 Tumor-Suppressor. *Biochemistry 34*, 5309−5316.
(34) Thompson, K. S., Vinson, C. R., and Freire, E. (1993) Thermodynamic Characterization of the Structural Stability of the Coiled-Coil Region of the Bzip Transcription Factor Gcn4. *Biochemistry 32*, 5491−5496.
(35) Freire, E. (1989) Statistical Thermodynamic Analysis of the Heat Capacity Function Associated with Protein Folding-Unfolding Transitions. *Comments Mol. Cell. Biophys. 6*, 123−140.
(36) Privalov, P. L., Khechinashvili, N. N., and Atanasov, B. P. (1971) Thermodynamic analysis of thermal transitions in globular proteins. I. Calorimetric study of chymotrypsinogen, ribonuclease and myoglobin. *Biopolymers 10*, 1865−1890.
(37) Freire, E., and Biltonen, R. L. (1978) Statistical Mechanical Deconvolution of Thermal Transitions in Macromolecules 0.1. Theory and Application to Homogeneous Systems. *Biopolymers 17*, 463−479.
(38) Vertrees, J., Barritt, P., Whitten, S., and Hilser, V. J. (2005) COREX/BEST server: a web browser-based program that calculates regional stability variations within protein structures. *Bioinformatics 21*, 3318−3319.
(39) Hilser, V. J., Garcia-Moreno, E. B., Oas, T. G., Kapp, G., and Whitten, S. T. (2006) A statistical thermodynamic model of the protein ensemble. *Chem. Rev. 106*, 1545−1558.
(40) D'Aquino, J. A., Gomez, J., Hilser, V. J., Lee, K. H., Amzel, L. M., and Freire, E. (1996) The magnitude of the backbone conformational entropy change in protein folding. *Proteins: Struct., Funct., Genet. 25*, 143−156.
(41) Gomez, J., and Freire, E. (1995) Thermodynamic mapping of the inhibitor site of the aspartic protease endothiapepsin. *J. Mol. Biol. 252*, 337−350.
(42) Gomez, J., Hilser, V. J., Xie, D., and Freire, E. (1995) The heat capacity of proteins. *Proteins: Struct., Funct., Genet. 22*, 404−412.
(43) Xie, D., and Freire, E. (1994) Molecular basis of cooperativity in protein folding. V. Thermodynamic and structural conditions for the stabilization of compact denatured states. *Proteins: Struct., Funct., Genet. 19*, 291−301.
(44) Murphy, K. P., Bhakuni, V., Xie, D., and Freire, E. (1992) Molecular basis of co-operativity in protein folding. III. Structural identification of cooperative folding units and folding intermediates. *J. Mol. Biol. 227*, 293−306.
(45) Xie, D., and Freire, E. (1994) Structure based prediction of protein folding intermediates. *J. Mol. Biol. 242*, 62−80.
(46) Baldwin, R. L. (1986) Temperature dependence of the hydrophobic interaction in protein folding. *Proc. Natl. Acad. Sci. U. S. A. 83*, 8069−8072.
(47) Liu, T., Pantazatos, D., Li, S., Hamuro, Y., Hilser, V. J., and Woods, V. L., Jr. (2012) Quantitative assessment of protein structural models by comparison of H/D exchange MS data with exchange behavior accurately predicted by DXCOREX. *J. Am. Soc. Mass Spectrom. 23*, 43−56.
(48) O'Shea, E. K., Rutkowski, R., and Kim, P. S. (1989) Evidence that the leucine zipper is a coiled coil. *Science 243*, 538−542.
(49) Day, C. L., and Alber, T. (2000) Crystal structure of the amino-terminal coiled-coil domain of the APC tumor suppressor. *J. Mol. Biol. 301*, 147−156.
(50) Holtzer, M. E., Lovett, E. G., d'Avignon, D. A., and Holtzer, A. (1997) Thermal unfolding in a GCN4-like leucine zipper: 13C alpha NMR chemical shifts and local unfolding curves. *Biophys. J. 73*, 1031−1041.
(51) Pettersen, E. F., Goddard, T. D., Huang, C. C., Couch, G. S., Greenblatt, D. M., Meng, E. C., and Ferrin, T. E. (2004) UCSF Chimera–a visualization system for exploratory research and analysis. *J. Comput. Chem. 25*, 1605−1612.
(52) Oakley, M. G., and Kim, P. S. (1998) A buried polar interaction can direct the relative orientation of helices in a coiled coil. *Biochemistry 37*, 12603−12610.
(53) Boyken, S. E., Chen, Z., Groves, B., Langan, R. A., Oberdorfer, G., Ford, A., Gilmore, J. M., Xu, C., DiMaio, F., Pereira, J. H., Sankaran, B., Seelig, G., Zwart, P. H., and Baker, D. (2016) De novo design of protein homo-oligomers with modular hydrogen-bond network-mediated specificity. *Science 352*, 680−687.
(54) Lee, K. H., Xie, D., Freire, E., and Amzel, L. M. (1994) Estimation of changes in side chain configurational entropy in binding and folding: general methods and application to helix formation. *Proteins: Struct., Funct., Genet. 20*, 68−84.
(55) Murphy, K. P., Xie, D., Thompson, K. S., Amzel, L. M., and Freire, E. (1994) Entropy in biological binding processes: estimation of translational entropy loss. *Proteins: Struct., Funct., Genet. 18*, 63−67.
(56) Ulmschneider, B., Grillo-Hill, B. K., Benitez, M., Azimova, D. R., Barber, D. L., and Nystul, T. G. (2016) Increased intracellular pH is necessary for adult epithelial and embryonic stem cell differentiation. *J. Cell Biol. 215*, 345−355.

DOI: 10.1021/acs.biochem.7b00469
Biochemistry 2017, 56, 4646−4655

(57) Putney, L. K., and Barber, D. L. (2003) Na-H exchange-dependent increase in intracellular pH times G2/M entry and transition. *J. Biol. Chem. 278*, 44645−44649.
(58) Perez-Sala, D., Collado-Escobar, D., and Mollinedo, F. (1995) Intracellular alkalinization suppresses lovastatin-induced apoptosis in HL-60 cells through the inactivation of a pH-dependent endonuclease. *J. Biol. Chem. 270*, 6235−6242.
(59) Webb, B. A., Chimenti, M., Jacobson, M. P., and Barber, D. L. (2011) Dysregulated pH: a perfect storm for cancer progression. *Nat. Rev. Cancer 11*, 671−677.
(60) Nilsson, C., Johansson, U., Johansson, A. C., Kagedal, K., and Ollinger, K. (2006) Cytosolic acidification and lysosomal alkalinization during TNF-alpha induced apoptosis in U937 cells. *Apoptosis 11*, 1149−1159.
(61) Barry, M. A., and Eastman, A. (1992) Endonuclease activation during apoptosis: the role of cytosolic Ca2+ and pH. *Biochem. Biophys. Res. Commun. 186*, 782−789.
(62) Amit, I., Yakir, L., Katz, M., Zwang, Y., Marmor, M. D., Citri, A., Shtiegman, K., Alroy, I., Tuvia, S., Reiss, Y., Roubini, E., Cohen, M., Wides, R., Bacharach, E., Schubert, U., and Yarden, Y. (2004) Tal, a Tsg101-specific E3 ubiquitin ligase, regulates receptor endocytosis and retrovirus budding. *Genes Dev. 18*, 1737−1752.
(63) Kim, B. Y., Olzmann, J. A., Barsh, G. S., Chin, L. S., and Li, L. (2007) Spongiform neurodegeneration-associated E3 ligase Mahogunin ubiquitylates TSG101 and regulates endosomal trafficking. *Mol. Biol. Cell 18*, 1129−1142.
(64) Im, Y. J., Kuo, L., Ren, X. F., Burgos, P. V., Zhao, X. Z., Liu, F., Burke, T. R., Bonifacino, J. S., Freed, E. O., and Hurley, J. H. (2010) Crystallographic and Functional Analysis of the ESCRT-I/HIV-1 Gag PTAP Interaction. *Structure 18*, 1536−1547.
(65) Pornillos, O., Alam, S. L., Rich, R. L., Myszka, D. G., Davis, D. R., and Sundquist, W. I. (2002) Structure and functional interactions of the Tsg101 UEV domain. *EMBO J 21*, 2397−2406.
(66) Pornillos, O., Higginson, D. S., Stray, K. M., Fisher, R. D., Garrus, J. E., Payne, M., He, G. P., Wang, H. E., Morham, S. G., and Sundquist, W. I. (2003) HIV Gag mimics the Tsg101-recruiting activity of the human Hrs protein. *J. Cell Biol. 162*, 425−434.
(67) Lu, Q., Hope, L. W., Brasch, M., Reinhard, C., and Cohen, S. N. (2003) TSG101 interaction with HRS mediates endosomal trafficking and receptor down-regulation. *Proc. Natl. Acad. Sci. U. S. A. 100*, 7626−7631.
(68) Sundquist, W. I., Schubert, H. L., Kelly, B. N., Hill, G. C., Holton, J. M., and Hill, C. P. (2004) Ubiquitin recognition by the human TSG101 protein. *Mol. Cell 13*, 783−789.
(69) Allen, W. J., Balius, T. E., Mukherjee, S., Brozell, S. R., Moustakas, D. T., Lang, P. T., Case, D. A., Kuntz, I. D., and Rizzo, R. C. (2015) DOCK 6: Impact of new features and current docking performance. *J. Comput. Chem. 36*, 1132−1156.
(70) Kostelansky, M. S., Sun, J., Lee, S., Kim, J., Ghirlando, R., Hierro, A., Emr, S. D., and Hurley, J. H. (2006) Structural and functional organization of the ESCRT-I trafficking complex. *Cell 125*, 113−126.

DOI: 10.1021/acs.biochem.7b00469
Biochemistry 2017, 56, 4646−4655